Collision-Energy-Resolved Penning Ionization Electron Spectroscopy of Difluorobenzenes: Anisotropic Interaction of Difluorobenzenes with He*(2^3S) and Assignments of Ionic States

Kohei Imura, Naoki Kishimoto, and Koichi Ohno*

Department of Chemistry, Graduate School of Science, Tohoku University, Aramaki, Aoba-ku, Sendai 980-8578, Japan

Received: February 7, 2001

Penning ionization of difluorobenzenes upon collision with metastable He*(2^3S) atoms was studied by two-dimensional (collision-energy/electron-energy-resolved) Penning ionization electron spectroscopy. Collision energy dependence of the partial ionization cross sections (CEDPICS), which reflects interaction potential energy between the molecule and He*(2^3S), showed anisotropic interaction around the molecules. Assignments of the Penning ionization electron spectra and He I ultraviolet photoelectron spectra were discussed on the basis of different behavior of CEDPICS and calculated ionization potentials by the outer valence Green's function (OVGF) method. Furthermore, the ordering of the reactivity of the $n_{\parallel}$ and σ_{CF} orbitals and the magnitude of attractive interaction around the F atoms with the metastable atom was found to be *o*- > *m*- ∼ *p*-$C_6H_4F_2$. It indicates that the wider potential well brings the larger attractive effect for Penning ionization reaction.

I. Introduction

To elucidate a chemical reaction, it is important to investigate the dynamics of particles on the anisotropic interaction potential energy surface. A chemiionization process known as Penning ionization[1] occurs when a molecule M collides with a metastable atom A*, where A* has a larger excitation energy than the lowest ionization potential of M

$$A^* + M \rightarrow A + M^+ + e^-$$

The Penning ionization process can be explained by the electron-exchange model, in which overlap of orbitals related to the electron exchange is required.[2] Ohno et al.[3,4] successfully applied the exterior electron density (EED) model to this process in order to account for experimental branching ratios of Penning ionization. On the basis of this model, partial ionization cross-section can be roughly simulated by the EED, electron distribution of the target molecular orbitals (MOs) exposed outside the molecular surface, which is approximated by van der Waals radii. Then, larger electron distribution outside the molecular surface brings larger overlap of mutual orbitals involving electron exchange with resultant large ionization probability. Since target MOs have anisotropic electron distributions, the reaction probability also depends on anisotropy of the interaction potentials. Thus, Penning ionization electron kinetic energy spectrum (PIES) provides us information on the electron distribution of the target MOs exposed outside the boundary surface of collision.

It is obvious that the ionization cross-section depends not only on both the characteristic of the interaction between the colliding particles but also the collision energy of the particles. If the ionization reaction is mostly governed by the attractive interaction, the ionization cross section should enhance at lower collision energies, because a slower He* atom can approach the reactive region effectively. On the contrary, if the ionization reaction is mostly governed by the repulsive interaction, the ionization cross section should enhance at higher collision energies, because a faster He* atom can approach the reactive region more effectively. Therefore, observation of collision energy dependent cross section provides valuable information about the interaction potential energy surface. Two-dimensional PIES (2D-PIES) has been recently developed in our laboratory,[5] in which ionization cross sections are determined as functions of both electron kinetic energy (E_e) and collision energy (E_c). This technique makes it possible to study the collision energy dependence of the partial ionization cross-sections (CEDPICS) and collision-energy-resolved PIES (CERPIES), and thus, the state-resolved measurement of partial cross sections for the *i*th ionic state enable us to investigate anisotropic potential surface around the target molecule. 2D-PIES studies of several aromatic compounds (such as benzene,[6] polycyclic aromatic hydrocarbons,[7] heterocyclic compounds,[8] [2,2]paracyclophane,[9] azines,[10] substituted benzenes[11] (aniline, phenol, thiophenol), and monohalogenobenzenes[12]) with He(2^3S) atoms have been reported so far. By using the 2D-PIES characteristics, we proposed new band assignments of He I UPS and He*(2^3S) PIES for monofluorobenzene,[12] which are different from the past PIES study of Fujisawa et al.[13] Thus, these 2D-PIES studies were found to be useful for assigning photoelectron spectra of fluorine atom containing compounds.

Photoelectron spectra of difluorobenzenes have been extensively investigated.[14−22] However, there has been no attempt to assign the photoelectron spectrum of any of the difluorebenzenes except for refs 18 and 22, in which the observed bands were assigned on the basis of semiempirical MO calculation and Koopmans' theorem. Although Aoyama[23] studied PIES of these compounds and proposed band assignments, these assignments should be revised by the aid of the 2D-PIES characteristics.

In this paper, we have measured 2D-PIES of *o*-, *m*-, and *p*-$C_6H_4F_2$ in order to obtain an insight into the anisotropic interaction around the molecules and also to investigate the

10.1021/jp010477c CCC: $20.00
Published on Web 06/02/2001

substituent effect on the reactivity and anisotropic interactions with the He* atom for these compounds. In addition, assignments of observed bands by He I ultraviolet photoelectron spectroscopy were made on the basis of present experiments and calculations.

II. Experimental Section

High-purity samples *o*-, *m*-, and *p*-$C_6H_4F_2$ were commercially purchased and purified by several freeze−pump−thawed cycles. The experimental apparatus for He*(2^3S) Penning ionization electron spectroscopy has been reported previously.[6,24−26] The metastable He* beam was generated by a discharge nozzle source with a tantalum hollow cathode. The metastable He* atoms in the 2^1S state are optically removed by a helium discharge (quench) lamp after passing through a skimmer. Ionic and Rydberg species produced by the discharge were removed by an electric deflector. The He*(2^3S) metastable beam enters into the collision cell where sample gas was introduced. Produced electrons by the Penning ionization were measured by a hemispherical electrostatic deflection type analyzer using an electron collection angle 90° to the incident He* beam. He I UPS were measured by using the He I resonance photons (584 nm, 21.22 eV) produced by dc-discharge in pure helium gas. The kinetic energy of ejected electrons was measured by the analyzer using an electron collection angle 90° to the incident photon beam. The energy resolution of the electron energy analyzer was estimated to be 70 meV from the full width at the half-maximum (fwhm) of the $Ar^+(^2P_{3/2})$ peak in the He I UPS. The transmission efficiency curve of the electron analyzer was determined by comparing our UPS data of several molecules with those by Gardner and Samson[27] and Kimura et al.[28] Calibration of the electron energy scale was made by reference to the lowest ionic state of N_2 mixed with the sample molecule in He I UPS ($E_e = 5.639$ eV)[29] and He* (2^3S) PIES ($E_e = 4.292$ eV).[30,31]

In the collision-energy-resolved experiments, 2D-PIES, the metastable atom beam was modulated by a pseudorandom chopper[32] rotating about 400 Hz and introduced into the reaction cell located at 504 mm downstream from the chopper disk with sample pressure kept constant. The resolution of the electron analyzer was lowered to 250 meV in order to gain higher electron counting rates. Time-dependent electron signals for each kinetic electron energy (E_e) were recorded with scanning electron energy of a 35 meV step. The 2D Penning ionization data as functions of both E_e and t were stored in a memory of a computer. The velocity dependence of the electron signals was obtained from the time dependent signals by Hadamard transformation in which time dependent signals were cross-correlated with the complementary slit sequence of the pseudo-random chopper. Similarly, velocity distribution of metastable He* beam was determined by measuring the intensity of secondary emitted electrons from the inserted stainless plate. The 2D Penning ionization cross section $\sigma(E_e, v_r)$ was obtained with normalization by the velocity distribution of He* $I_{He^*}(v_{He^*})$

$$\sigma(E_e, v_r) = A[I_e(E_e, v_{He^*})/I_{He^*}(v_{He^*})](v_{He^*}/v_r)$$

$$v_r = [v_{He^*}^2 + 3kT/M]^{1/2}$$

where A, v_t, k, T, and M are proportionality constants, the relative velocity of metastable atoms averaged over the velocity of the sample molecule, the Boltzmann constants, the gas temperature (300 K), and the mass of the sample molecule, respectively. Finally, $\sigma(E_e, v_r)$ is converted to $\sigma(E_e, E_c)$ as functions of E_e and E_c by the following relation

$$E_c = \mu v_r^2/2$$

where μ is the reduced mass of the reaction system.

III. Calculations

We performed ab initio self-consistent field (SCF) calculations with 4-31G basis functions for *o*-, *m*-, and *p*-$C_6H_4F_2$ in order to obtain electron density contour maps of MOs. The geometries of the molecules were taken from microwave spectroscopic studies.[33,34] In electron density maps, thick solid curves indicate the repulsive molecular surface approximated by van der Waals radii[35] ($r_C = 1.7$ Å, $r_H = 1.2$ Å, $r_F = 1.35$ Å).

Interaction potential energies between He*(2^3S) and M in various directions and angles were also calculated on the basis of the well-known resemblance between He*(2^3S) and Li(2^2S);[36] the shape of the velocity dependence of the total scattering cross-section of He*(2^3S) by He, Ar, and Kr is very similar to that of Li, and the location of the interaction potential well and its depth are similar for He*(2^3S) and Li with various targets.[37−40] Because of these findings and the difficulties associated with calculation for excited states, the Li was used in this study in place of He*(2^3S). Thus, the interaction potential M−Li(2^2S), $V^*(R,\theta)$ (where R is the distance between Li atom and either F atom or the center of the benzene ring and θ is in-plane angle defined in Figures 10b, 11b, and 12b) was calculated by moving the Li atom toward halogen atom and keeping the molecular geometries fixed at the experimental values; this assumption meant that the geometry change by the approach of a metastable atom was negligible in the collisional ionization process. For calculating the interaction potential, standard 6-31+G* basis set was used, and the correlation energy correction was partially taken into account by using second-order Møller−Plesset perturbation theory (MP2). All the calculations in this study were performed with the GAUSSIAN 98 quantum chemistry program.[41] The ionization potentials were calculated at the experimentally determined geometries using the outer valence Green's function (OVGF) method[42,43] for *o*-, *m*-, and *p*-$C_6H_4F_2$ with 6-311G** basis sets as incorporated in GAUSSIAN 98.

IV. Results

Figures 1−3 show the He I UPS and He*(2^3S) PIES of *o*-, *m*-, and *p*-$C_6H_4F_2$. The electron energy scale for PIES are shifted relative to those of UPS by the excitation energy difference between He I photons (21.22 eV) and He*(2^3S) (19.82 eV), namely, 1.40 eV. The assignments of the He I UPS and He*(2^3S) will be discussed in a later section. Band labels in UPS show orbital characters on the basis of their symmetries and the latter definitions.

Figures 4−6 show the collision-energy-resolved PIES (CER-PIES) obtained from the 2D spectra of *o*-, *m*-, and *p*-$C_6H_4F_2$. Hot spectra at the higher collision energy (ca. 250 meV) are shown by dashed curves, and the cold ones at the lower collision energy (ca. 100 meV) are shown by solid curves. The relative intensities of the two spectra are normalized in the figures using the data of the log σ vs log E_c plots.

Figures 7−9 show the log σ versus log E_c plots of CEDPICS in a collision energy range of 90−300 meV for *o*-, *m*-, and *p*-$C_6H_4F_2$. The CEDPICS was obtained from the 2D-PIES $\sigma(E_e,E_c)$ within an appropriate range of E_e (typically electron energy resolution of analyzer, 250 meV) to avoid the contribution from neighbor bands. Electron density maps are also shown

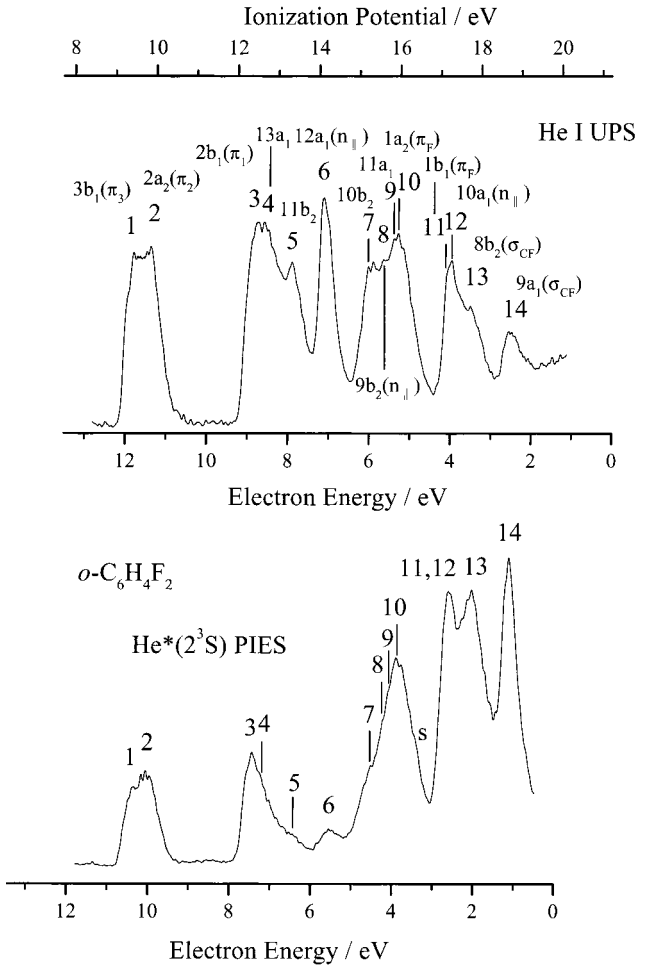

Figure 1. He I UPS and He(2^3S) PIES spectrum of *o*-$C_6H_4F_2$. Average collision energy (60−400 meV) of PIES was ∼160 meV.

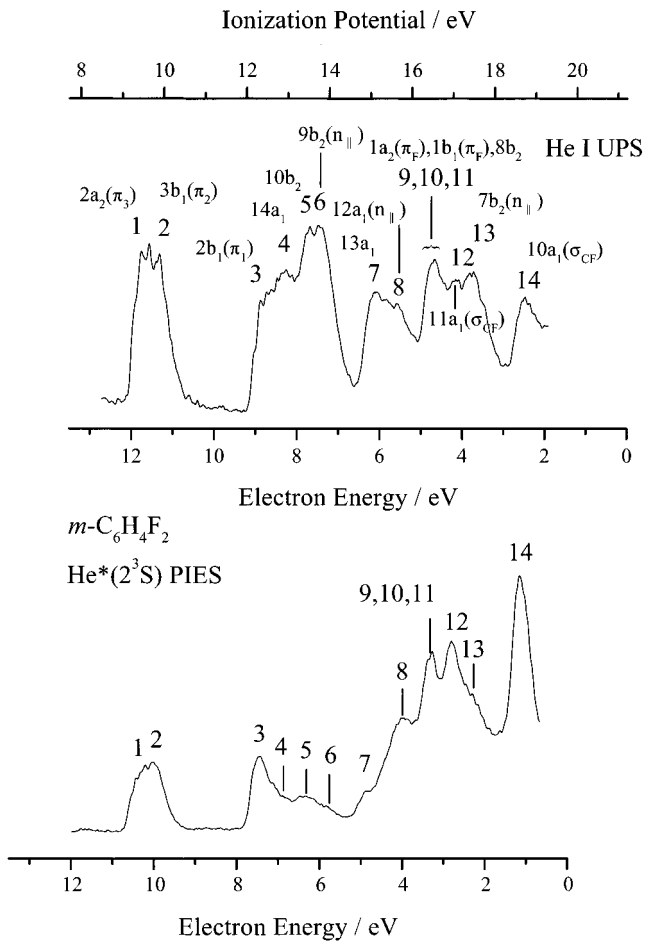

Figure 2. He I UPS and He(2^3S) PIES spectrum of *m*-$C_6H_4F_2$. Average collision energy (60−400 meV) of PIES was ∼160 meV.

in the figures in order to grasp effective access direction of He*. The calculated electron density maps for s orbitals are shown on the molecular plane, and those for p orbitals are shown on a plane at a height of 1.7 Å (van der Waals radii of C atom) from the molecular plane. At the right side of the figures, electron density maps for π_3, π_2, and π_1 orbitals were drawn on either the symmetry plane perpendicular to the molecular plane or a plane including the center of the benzene ring and being perpendicular to both the symmetry plane and the molecular plane. In addition, electron density maps for π_3, π_2, π_1, and π_F orbitals were drawn on a plane including both the F atom and the center of the benzene ring and being perpendicular to the molecular plane. Italic numbers and dashed curves for π_3, π_2, and π_1 orbitals will be defined later.

Figures 10−12 show calculated interaction potential energy curves between a ground-state Li atom and *o*-, *m*-, and *p*-$C_6H_4F_2$, respectively. The potential energy curves are shown as a function of (a) the distance R between Li and either the F atom or the center of the benzene ring, (b) the in-plane angle θ. Calculations were performed at the MP2/6-31+G* level of theory.

Tables 1−3 summarize experimentally observed and calculated ionization potentials (IPs), experimental peak energy shift (ΔE), slope parameters of CEDPICS (m), and the assignment of the bands. Slope parameters are obtained from the log σ vs log E_c plots in a collision energy range for 90−300 meV by a least-squares method. Vertical IPs are determined from He I UPS. The peak energy shifts are obtained as the difference between the peak position (E_{PIES}; electron energy scale) and the "nominal" value (E_0 = difference between metastable excitation energy and sample IP): $\Delta E = E_{PIES} - E_0$.

V. Discussion

Band Assignments and PIES Intensities. Photoelectron spectra of difluorobenzenes have been extensively investigated.[14−22] The major aim of these studies was to elucidate the structure of benzene itself and clarify the assignment of its photoelectron spectrum. The question of interest for these studies was the position of the first three π-bands, which derived from the splitting of $e_{1g}(\pi)$ orbitals and $a_{2u}(\pi)$ orbital of benzene. The first two bands in UPS of difluorobenzenes were unambiguously assigned as π_3 and π_2 orbitals, which result from the removal of degeneracy of the benzene $e_{1g}(\pi)$ orbitals due to substitution. There was also the question whether the first lowest IP associated with a σ-bonding type MO was lower than the third π band, π_1. This has not been definitely established so far, while von Nissen et al.[19] suggested that the two IPs were so close together that they were regarded as equal. There has been no attempt to assign the photoelectron spectrum of any of the difluorobenzenes experimentally except for the first lowest four IPs, a formidable task in view of numerous bands with energies between 9 and 21 eV and their overlap. One difficulty for assigning the spectra in this region can be ascribed to the fact that the atomic ionization potential of fluorine is higher than that of the other halogen substituents and the lone pair ionization of the aliphatic fluoride occur in the region 16−19 eV. In refs 18 and 22, assignment for some of the observed bands and sequence of the MOs energies related to the remaining

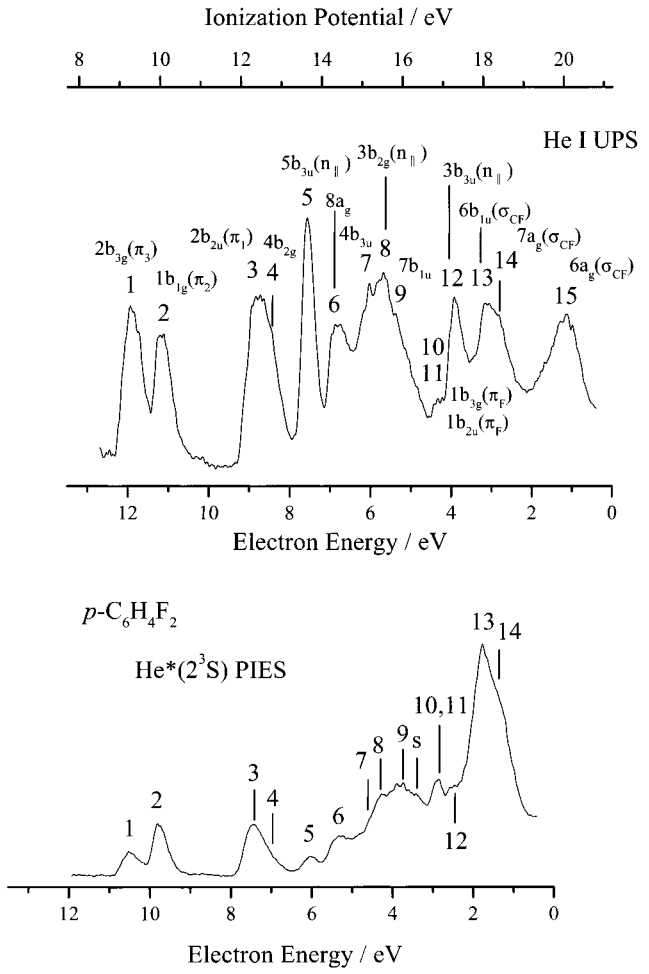

Figure 3. He I UPS and He(2^3S) PIES spectrum of *p*-$C_6H_4F_2$. Average collision energy (60−400 meV) of PIES was ∼160 meV.

bands was proposed on the basis of semiempirical MO calculation and the validity of Koopmans' theorem, while it is hard to say that the complete assignments of UPS for these compounds have been established.

Aoyama[23] studied PIES of these compounds and proposed their band assignments. However, as was mentioned in the Introduction, more careful assignments are necessary by taking the result of the 2D-PIES experiment and the similarity to the monofluorobenzene[12,13] into account. PIES for *o*-, *m*-, and *p*-$C_6H_4F_2$ are shown in Figures 1−3 together with UPS. The branching ratios are clearly different compared to those in UPS, which reflect the difference in the ionization mechanism; strong bands in PIES originate from orbitals having large electron density exposed outside to the molecular surface. By using this feature of PIES together with measuring the collision-energy-resolved PIES shown in Figures 4−6, π_1 and the first σ type orbitals could be clearly assigned. We assigned the stronger peak appeared at E_e ∼7.5 eV (band 3) to ionization from the π_1 orbital and the weak shoulder appeared at E_e ∼7.0 eV (band 4) to σ_{CH} type MO for these compounds, since it has been reported that the $\pi_{3,2,1}$ orbitals give strong PIES intensities being similar to the case of monofluorobenzene[12,13] and the σ_{CH} orbital shows the smaller PIES intensity.[44] Sharp peaks around IP ∼14 eV in UPS shown in Figures 1−3 are typical observation due to ionization from nonbonding MOs. In the case of monofluorobenzene,[12,13] corresponding peak was observed at IP = 13.90 eV in UPS and assigned as $n_{||}$ (nonbonding orbital mostly due to fluorine 2p orbital directed perpendicular to the C−F bond axis distributed in-plane to the benzene ring) orbital. Then, we

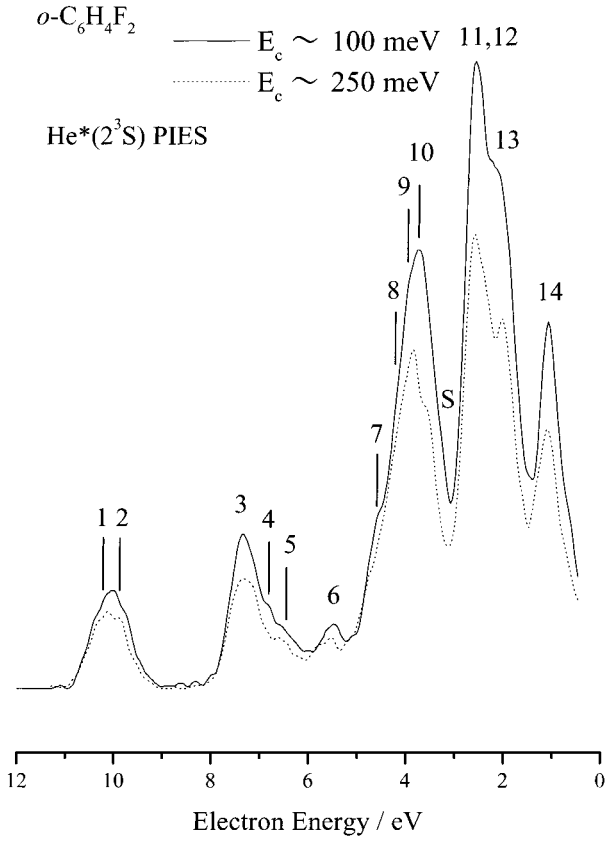

Figure 4. Collision-energy-resolved He(2^3S) PIES of *o*-$C_6H_4F_2$. E_c denotes collision energy.

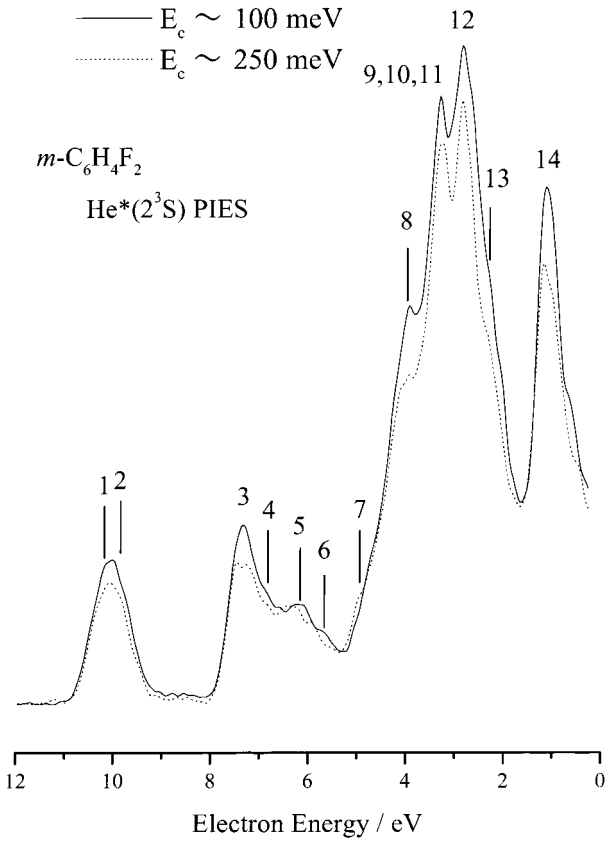

Figure 5. Collision-energy-resolved He(2^3S) PIES of *m*-$C_6H_4F_2$. E_c denotes collision energy.

related them (bands 6 for *o*-, *m*-$C_6H_4F_2$ and band 5 for *p*-$C_6H_4F_2$) to the ionization from $n_{||}$ orbitals. In PIES, these $n_{||}$ bands of

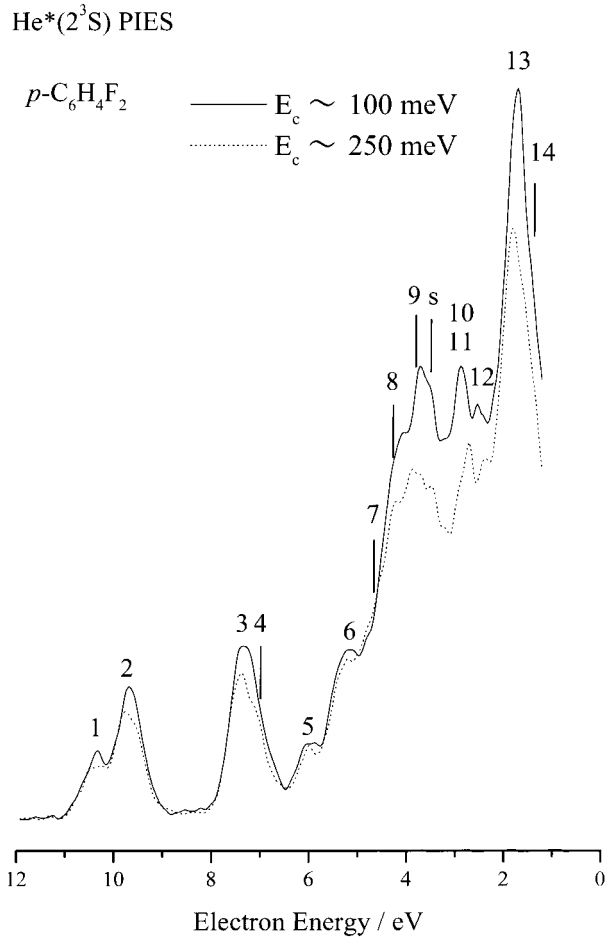

Figure 6. Collision-energy-resolved He(2^3S) PIES of *p*-$C_6H_4F_2$. E_c denotes collision energy.

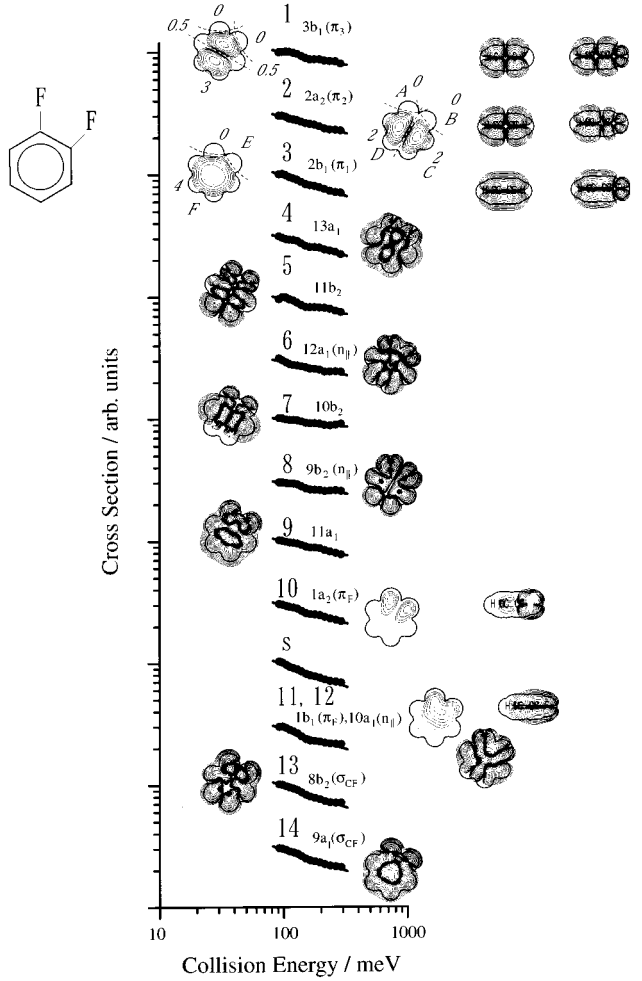

Figure 7. Collision energy dependence of partial ionization cross sections for *o*-$C_6H_4F_2$ with He(2^3S) atom. The contour plots show electron density maps for respective MOs. Italic numbers are defined in the text. Nodal planes are schematically drawn as dashed curves.

difluorobenzenes were observed as weak peaks as the case of monofluorobenzene.[12,13] Weak PIES intensities for these bands can be explained from a steric shielding effect of the benzene ring. Namely, the benzene ring spatially prevents reactive trajectories of He* toward F atoms with resultant smaller ionization probability. It is known that such a shielding effect of bulky groups has been found in various compounds.[45−47] In PIES of monofluorobenzne,[12,13] very strong peak assigned as σ_{CF} orbital was observed at E_e ~2.0 eV. (σ_{CF} is bonding orbital mostly due to fluorine 2p orbital with the collinear direction to the C−F bond axis.) In accord with this observation, very strong peaks were observed near the corresponding region at E_e ~3.0−1.0 eV for difluorobenzenes. We related these strong peaks (bands 13 and 14 for *o*-, *p*-$C_6H_4F_2$ and bands 12 and 14 for *m*-$C_6H_4F_2$) to ionization from MOs having a σ_{CF} orbital character. These strong PIES intensities are explained by large electron distribution exposed outside the repulsive surface as mentioned in the Introduction. π_F (out-of-plane fluorine 2p orbital conjugated with some of carbon 2p orbitals in benzene) band in PIES of monofluorobenzene[12,13] showed relatively strong PIES intensity around E_e ~4 eV. Being similar to the case of monofluorobenzene,[12,13] relatively strong intensity of difluorobenzenes around E_e ~4−3 eV were observed and assigned as two π_F bands, which are associated with the ungerade (u) and gerade (g) combinations of the F 2p orbitals (bands 10 and 11 for *o*-, *p*-$C_6H_4F_2$ and two of bands 9−11 for *p*-$C_6H_4F_2$) based both on the OVGF calculations and on the latter discussions. A general feature of the PIES of the investigated molecules together with monofluorobenzene can be summarized as follows:

In monofluorobenzene, $I(\sigma_{CF}) \gg I(\pi_{3,2,1})$, $I(\pi_F) > I(n_{||}) > I(\sigma_{CC})$, $I(\sigma_{CH})$.

In difluorobenzenes, $I(\sigma_{CF}) \geq I(\pi_F) \geq I(\pi_{3,2,1}) > I(n_{||}) > I(\sigma_{CC})$, $I(\sigma_{CH})$.

Similar MO reactivity with He*(2^3S) was found between monofluorobenzene and difluorobenzenes. Peak energy shifts in PIES are not clearly observed for several bands because of band overlap and relatively large bandwidth in PIES.

Collision Energy Dependence of the Partial Ionization Cross-Sections (CEDPICS). (i) General Feature of CEDPICS. Strong negative collision energy dependence of the partial ionization cross-section was observed for $\pi_{3,2,1}$, π_F, and σ_{CF} bands. It implies that the ionization for these bands governed by the attractive interaction with He*. When a slower He* metastable atom can approach the reactive region effectively by attractive force, ionization cross section is enhanced for lower collision energies. In case of *m*- and *p*-$C_6H_4F_2$, slightly smaller absolute values of CEDPICS for $n_{||}$ bands (band 6 of *m*-$C_6H_4F_2$ and 5 of *p*-$C_6H_4F_2$) than that of $\pi_{3,2,1}$, π_F, and σ_{CF} band were found, while in the case of *o*-$C_6H_4F_2$ slightly small slope parameter of CEDPICS for $n_{||}$ band (band 6) than that of $\pi_{3,2,1}$, π_F, and σ_{CF} band was obtained. The smallest absolute slope values of CEDPICS for bands 7 appeared around E_e ~4.5−5.0 eV in PIES among these compounds was found, and it indicates that ionization event from this MO is governed by stronger repulsive interaction around the C−H bonds with the He* atom

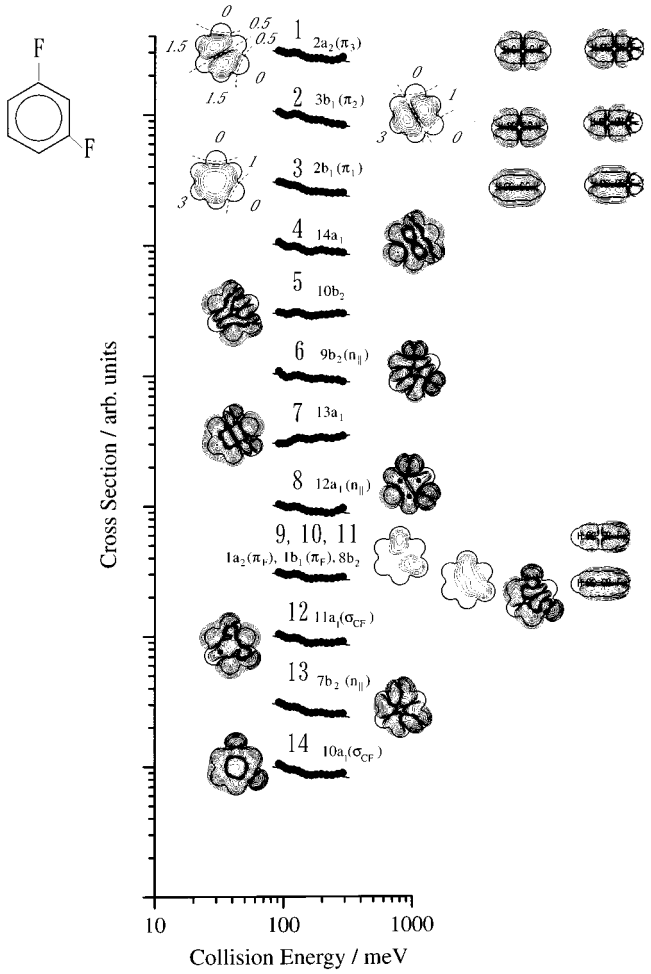

Figure 8. Collision energy dependence of partial ionization cross sections for *m*-$C_6H_4F_2$ with He(2^3S) atom. The contour plots show electron density maps for respective MOs. Italic numbers are defined in the text. Nodal planes are schematically drawn as dashed curves.

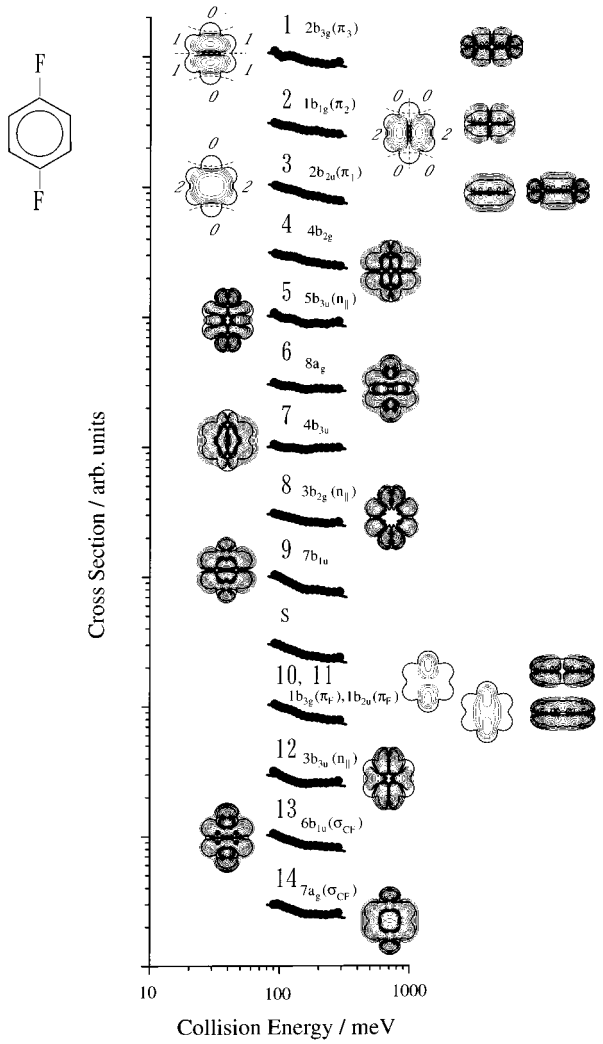

Figure 9. Collision energy dependence of partial ionization cross sections for *p*-$C_6H_4F_2$ with He(2^3S) atom. The contour plots show electron density maps for respective MOs. Italic numbers are defined in the text. Nodal planes are schematically drawn as dashed curves.

compared to the other MOs. This is consistent with the relatively weak PIES intensity of this band. Then we assigned bands 7 to ionization from $10b_2$, $13a_1$, and $4b_{3u}$ σ-type orbital for *o*-, *m*-, and *p*-$C_6H_4F_2$, respectively. It is noted that either positive (+0.10) or small (−0.03) value of slope parameter of CEDPICS for band 7 was observed in the case of *m*- and *p*-$C_6H_4F_2$, while slightly larger (−0.12) absolute value of slope was observed in the case of *o*-$C_6H_4F_2$. It implies that the He* atoms approach around the F atoms was effectively shielded by the benzene ring for *m*- and *p*- than the case for *o*-$C_6H_4F_2$. This difference can be raised from a wider potential well for *o*-$C_6H_4F_2$ as can be seen in Figures 10b−12b. Briefly, we summarized the ordering of slope of CEDPICS for each band among these compounds as follows:

In C_6H_5F, $m(\pi_{3,2,1})$, $m(\pi_F)$, $m(\sigma_{CF}) < m(n_{||}) < m(\sigma_{CH})$.

In *o*-, *m*-, and *p*-$C_6H_4F_2$, $m(\pi_{3,2,1})$, $m(\pi_F)$, $m(\sigma_{CF}) \leq m(n_{||}) < m(\sigma_{CH})$.

It is important to realize that absolute slope value of CEDPICS for each band for *o*-$C_6H_4F_2$ is larger than that of corresponding band for *m*- and *p*-$C_6H_4F_2$, while the above summarized orderings of slope of CEDPICS for each band among these compounds are almost equivalent. This finding indicates that reactivity of *o*-$C_6H_4F_2$ is different from the others *m*- and *p*-$C_6H_4F_2$. The reason for this behavior will be discussed later.

Generally, a change in the degree of the slope parameters for the other bands among these compounds depends on the contribution of the attractive interaction around the F atom and the repulsive interaction around C−H bonds. For instance, electron distributions of $11a_1$ and $8b_2(\sigma_{CF})$ orbitals for *o*-$C_6H_4F_2$ as shown in Figure 7 are very similar to each other except for electron distribution around the C−H bonds. Smaller absolute slope parameter (−0.23) of band 9 ($11a_1$) than that (−0.34) of band 13 ($8b_2(\sigma_{CF})$) can be responsible for larger repulsive effect around the C−H bonds for $11a_1$ orbital than that for $8b_2(\sigma_{CF})$ orbital. We use this feature to assign the remaining bands, and further discuss the assignment and reactivity of the remaining bands for each compound below.

(ii) *o*-$C_6H_4F_2$. Smaller PIES intensity of band 5 compared with the other bands can be attributed to smaller electron distributions outside the repulsive surface, and band 5 was assigned as the $11b_2$ orbital. Bands 11 and 12 are seriously overlapped with each other in both UPS and PIES. CEDPICS of bands 11 and 12 as indicated in Figure 7 composed of two characters, one for lower collision energy region (E_c = 90−160 meV) and the other one for higher energy (E_c = 160−300 meV). It seems that the steep decrease of the partial ionization cross-section with increasing the collision energy for the lower region could be mainly attributed to ionization due to $1b_1(\pi_F)$ MO, since the CEDPICS for lower collision energy region was similar to that of band 10, which was assigned to $1a_2(\pi_F)$ orbital.

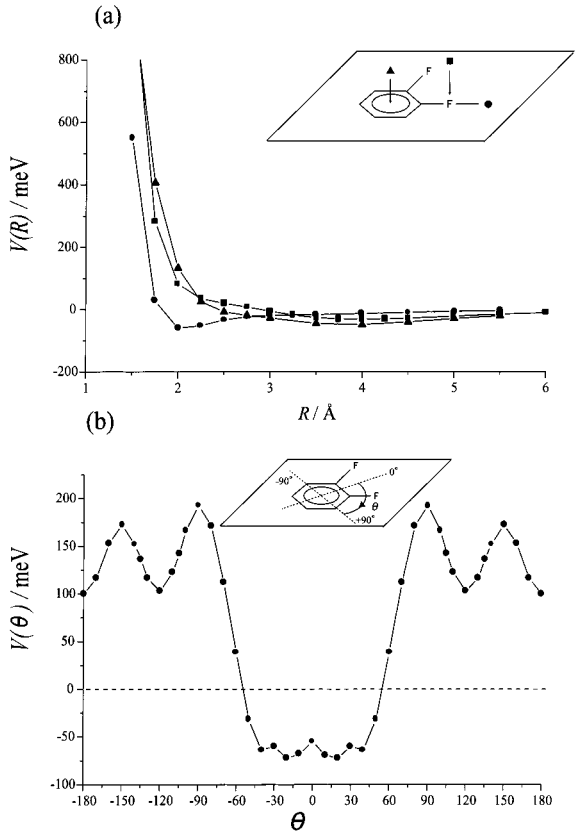

Figure 10. (a) Interaction potential curves V(R) obtained by MP2 calculations for *o*-$C_6H_4F_2$ and Li as a function of distance R; out-of-plane access to the center of the benzene ring (▲); in-plane collinear access to the C−F bond (●); out-of-plane perpendicular access to the C−F bond (■). Note that R is defined from the center of the benzene ring for (▲) direction, while for the others (●), (■) R is defined from the F atom. (b) Interaction potential curve $V(\theta)$ as a function of the in-plane angle θ. Distance between Li and the center of benzene ring is fixed at 4.71 Å. Note that the distance between the Li and F atoms at $\theta = \pm 30°$ is 2.0 Å.

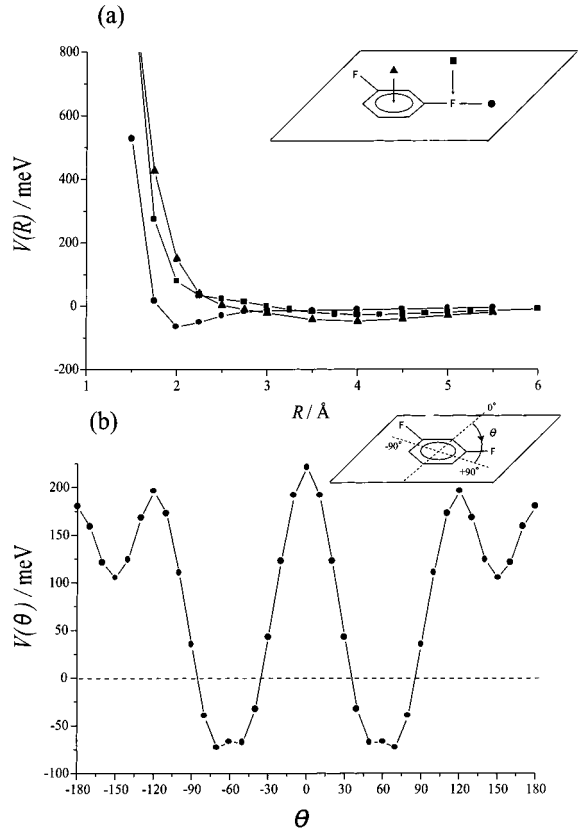

Figure 11. (a) Interaction potential curves V(R) obtained by MP2 calculations for *m*-$C_6H_4F_2$ and Li as a function of distance R; out-of-plane access to the center of the benzene ring (▲); in-plane collinear access to the C−F bond (●); out-of-plane perpendicular access to the C−F bond (■). Note that R is defined from the center of the benzene ring for (▲) direction, while for the others (●), (■) R is defined from the F atom. (b) Interaction potential curve $V(\theta)$ as a function of the in-plane angle θ. Distance between Li and the center of benzene ring is fixed at 4.71 Å. Note that the distance between the Li and F atoms at $\theta = \pm 60°$ is 2.0 Å.

On the other hand, the CEDPICS for higher collision energy region could be related to $10a_1(n_{||})$ orbital, since the CEDPICS for higher region was almost equivalent to that of the other $n_{||}$ bands. It may be puzzling here, since $n_{||}$ orbital does not give stronger PIES intensity. However, very strong PIES intensity of band 11,12 can be mainly attributed to the contribution from the π_F orbital since this MO has larger electron distribution exposed outside the molecular surface as indicated in Figure 7. The other π_F orbital (band 10) also shows very strong PIES intensity. Moreover, similar slope parameter of CEDPICS for bands 10 (−0.29) and 11,12 (−0.33) is consistent with major contribution of $1b_1(\pi_F)$ MO to band 11,12. Remaining band 8 is related to $9b_2(n_{||})$ orbital based on the OVGF calculation.

Although it is not clearly seen in PIES for this molecule, it has been reported that the configuration interaction (CI) band was observed for benzene[6] and some substituted benzene molecules.[48] This CI band was assigned to the ionization from the $\pi(1e_{1g})$ orbitals associated with the excitation from the $\pi(1e_{1g})$ orbitals to the $\pi^*(1e_{2u})$ orbitals,[49] since the binding energy for this CI band (16.1 eV) was in good agreement with the summation of the IP for the $\pi(1e_{1g})$ electron (9.25 eV) and the excitation energy for the $\pi(1e_{1g})$-$\pi^*(1e_{2u})(^1A_{1g}-{}^1E_{1u})$ transition (6.95 eV).[50] Taking the similarity of the electronic structure in both benzene and *o*-$C_6H_4F_2$ molecules into account, the CI band in *o*-$C_6H_4F_2$ can be evaluated with assumption of the same origin as that in benzene, i.e., π ionization associated with $\pi-\pi^*$ excitation. On the basis of the above assumption, the CI band position (IP = 16.46 eV) was calculated as $\pi-\pi^*$ excitation energy (7.02 eV)[50] plus π ionization of the highest occupied π_3 orbital of *o*-$C_6H_4F_2$ (9.44 eV). Thus, we assigned a shoulder of band 10 positioned at $E_e = 3.36$ eV (IP = 16.46 eV) to the CI band, which is denoted as s in Figure 1.

(iii) *m*-$C_6H_4F_2$. The smaller PIES intensity of band 13 than band 12 ($11a_1(\sigma_{CF})$) can be ascribed to the smaller electron distribution outside the repulsive surface along the C−F band axis. In addition, the smaller slope parameter (−0.18) of CEDPICS for band 13 than that (−0.14) for band 12 implies that MO related to band 13 involves smaller electron distribution around C−H bonds than that of $11a_1(\sigma_{CF})$ orbital, which was related to band 12. $7b_2(n_{||})$ orbital has smaller electron distribution around C−H bonds than that of $11a_1(\sigma_{CF})$ orbital, and then band 13 was related to $7b_2(n_{||})$ orbital. Moreover, OVGF calculations predicted that the corresponding MO, $7b_2(n_{||})$, appeared near band 13. Bands 5 and 8 are related to $10b_2$ and $12a_1(n_{||})$ orbitals, respectively, since the OVGF calculation predicted that IPs of these orbitals appeared corresponding region to the observed ones within 0.1 eV. In addition, since the $10b_2$ orbital has larger electron distribution around the C−H bonds, absolute value of slope parameter of CEDPICS for band 5 became smaller compared to the other bands except for band 7 as expected. Moreover, electron distribution of $12a_1(n_{||})$ and $9b_2(n_{||})$ orbitals is quite similar to each other, as a result, quite similar value of slope parameter of CEDPICS for these bands

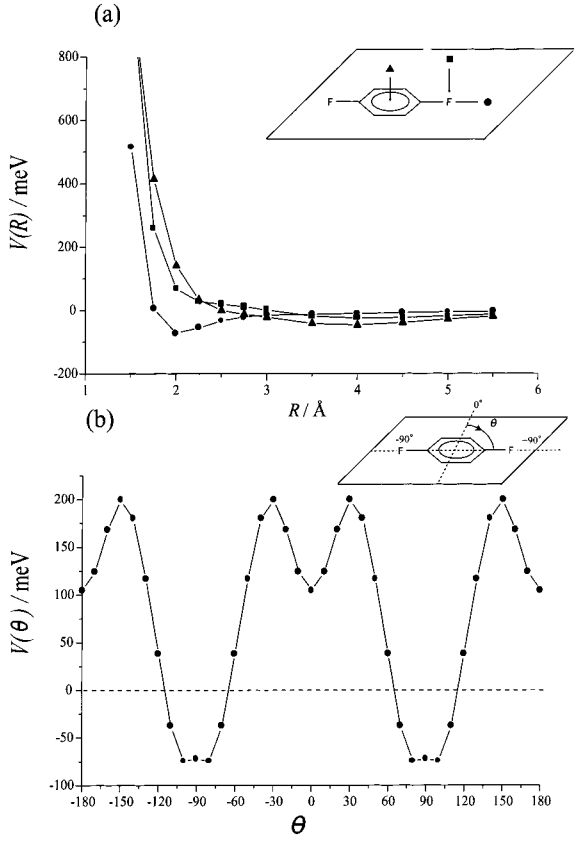

Figure 12. (a) Interaction potential curves V(R) obtained by MP2 calculations for p-$C_6H_4F_2$ and Li as a function of distance R; out-of-plane access to the center of the benzene ring (▲); in-plane collinear access to the C−F bond (●); out-of-plane perpendicular access to the C−F bond (■). Note that R is defined from the center of the benzene ring for (▲) direction, while for the others (●), (■) R is defined from the F atom. (b) Interaction potential curve $V(\theta)$ as a function of the in-plane angle θ. Distance between Li and the center of benzene ring is fixed at 4.71 Å. Note that the distance between the Li and F atoms at $\theta = \pm 90°$ is 2.0 Å.

TABLE 1: Band Assignment, Ionization Potentials (IP/eV), Peak Energy Shifts (ΔE/meV), and Slope Parameters (m) for o-$C_6H_4F_2$

molecule	band	IP_{obsd} (eV)	IP_{OVGF} (eV) (pole strength)	orbital character	ΔE (meV)	m
o-$C_6H_4F_2$	1	9.44	9.27(0.90)	$3b_1(\pi_3)$	−20 ± 70	−0.21
	2	9.86	9.61(0.90)	$2a_2(\pi_2)$	+50 ± 100	−0.27
	3	12.40	12.50(0.84)	$2b_1(\pi_1)$	+30 ± 100	−0.33
	4	12.64	12.83(0.90)	$13a_1$	+70 ± 100	−0.29
	5	13.33	13.24(0.90)	$11b_2$	(+100 ± 120)	−0.24
	6	14.11	14.15(0.89)	$12a_1(n_{\|\|})$	−160 ± 80	−0.22
	7	15.33	15.43(0.88)	$10b_2$	(0 ± 100)	−0.12
	8	15.58	15.48(0.89)	$9b_2(n_{\|\|})$	(+20 ± 80)	(−0.17)
	9	(15.84)	16.03(0.88)	$11a_1$	(+60 ± 120)	(−0.23)
	10	(15.94)	16.09(0.89)	$1a_2(\pi_F)$	(−10 ± 80)	(−0.29)
	11	(17.16)	16.80(0.85)	$1b_1(\pi_F)$	(−50 ± 100)	−0.33
	12	(17.27)	17.45(0.87)	$10a_1(n_{\|\|})$	(+60 ± 100)	
	13	17.72	17.91(0.87)	$8b_2(\sigma_{CF})$	−50 ± 70	−0.35
	14	18.67	18.82(0.87)	$9a_1(\sigma_{CF})$	−30 ± 70	−0.34
	s	16.46[a]				−0.35

[a] Obtained by He*(2^3S) PIES.

was observed. These observations further support the assignment of bands 5 and 8. For assigning bands 9−11, one cannot locate their origins in either UPS or PIES due to the overlapping of these bands. The theoretical values of IPs for these bands locate within 0.2 eV in very good agreement with experimental observation. Then, it was only possible to give the sequence of the MOs energies based on the calculation such as $1a_2(\pi_F)$, $1b_1(\pi_F)$, and $8b_2$, respectively. In PIES an overlapping band labeled by 9−11 shows very strong intensity because each of corresponding MOs has large electron distribution outside the repulsive surface. Moreover, $8b_2$ MO contains σ_{CF} type character, and then it is expected to give strong PIES intensity as the other σ_{CF} type orbitals.

TABLE 2: Band Assignment, Ionization Potentials (IP/eV), Peak Energy Shifts (ΔE/meV), and Slope Parameters (m) for m-$C_6H_4F_2$

molecule	band	IP_{obsd} (eV)	IP_{OVGF} (eV) (pole strength)	orbital character	ΔE (meV)	m
m-$C_6H_4F_2$	1	9.44	9.35(0.90)	$2a_2(\pi_3)$	−20 ± 60	−0.15
	2	9.80	9.61(0.90)	$3b_1(\pi_2)$	+60 ± 100	−0.20
	3	12.34	12.50(0.84)	$2b_1(\pi_1)$	+40 ± 70	−0.19
	4	12.96	13.00(0.90)	$14a_1$	(+90 ± 100)	−0.14
	5	13.45	13.48(0.90)	$10b_2$	(+80 ± 90)	−0.02
	6	13.72	13.87(0.89)	$9b_2$ ($n_{\|\|}$)	(−120 ± 120)	−0.11
	7	15.08	15.27(0.88)	$13a_1$	+80 ± 100	+0.10
	8	15.62	15.66(0.89)	$12a_1(n_{\|\|})$	−110 ± 100	−0.10
	9	(16.46)	16.32(0.89)	$1a_2(\pi_F)$		−0.09
	10	(16.53)	16.52(0.86)	$1b_1(\pi_F)$		
	11	(16.53)	16.56(0.88)	$8b_2$		
	12	17.0	17.25(0.87)	$11a_1(\sigma_{CF})$	+30 ± 120	−0.12
	13	17.40	17.55(0.88)	$7b_2(n_{\|\|})$	+20 ± 120	−0.18
	14	18.68	18.86(0.87)	$10a_1(\sigma_{CF})$	+50 ± 100	−0.14
	s	16.40[a]				

[a] Obtained by He*(2^3S) PIES.

TABLE 3: Band Assignment, Ionization Potentials (IP/eV), Peak Energy Shifts (ΔE/meV), and Slope Parameters (m) for p-$C_6H_4F_2$

molecule	band	IP_{obsd} (eV)	IP_{OVGF} (eV) (pole strength)	orbital character	ΔE (meV)	m
p-$C_6H_4F_2$	1	9.28	9.08(0.90)	$2b_{3g}(\pi_3)$	−10 ± 60	−0.18
	2	10.01	9.81(0.90)	$1b_{1g}(\pi_2)$	0 ± 70	−0.18
	3	12.38	12.43(0.84)	$2b_{2u}(\pi_1)$	−30 ± 60	−0.25
	4	12.70	12.59(0.90)	$4b_{2g}$	(+40 ± 120)	−0.20
	5	13.65	13.78(0.89)	$5b_{3u}(n_{\|\|})$	−110 ± 80	−0.14
	6	14.35	14.40(0.89)	$8a_g$	−50 ± 100	−0.09
	7	15.19	15.18(0.88)	$4b_{3u}$	(−40 ± 120)	−0.03
	8	15.53	15.58(0.89)	$3b_{2g}(n_{\|\|})$	−20 ± 90	−0.16
	9	15.83	15.73(0.88)	$7b_{1u}$	−80 ± 100	(−0.27)
	10	(16.85)	16.33(0.89)	$1b_{3g}(\pi_F)$	(0 ± 120)	−0.26
	11	(16.89)	16.44(0.86)	$1b_{2u}(\pi_F)$	(−80 ± 100)	
	12	17.28	17.46(0.87)	$3b_{3u}(n_{\|\|})$	(−40 ± 120)	(−0.15)
	13	18.05	18.18(0.88)	$6b_{1u}(\sigma_{CF})$	+10 ± 80	−0.21
	14	18.39	18.43(0.86)	$7a_g(\sigma_{CF})$	(−50 ± 120)	(−0.18)
	15	20.07	20.55(0.84)	$6a_g(\sigma_{CF})$		
	s	16.32[a]				(−0.24)

[a] Obtained by He*(2^3S) PIES.

(iv) p-$C_6H_4F_2$. As mentioned before, sharp peak in UPS is typically observed for the ionization from nonbonding-type MO. Then sharp peaks around IP ∼15.5 (band 8) and 17.3 eV (band 12) are related to ionization from $n_{||}$ orbitals. In PIES, these showed smaller intensity compared with neighboring bands as in the case of the other $n_{||}$ orbital (band 5). Furthermore, slope parameters (−0.14, −0.15) of CEDPICS for bands 8 and 12 are very similar to that (−0.14) for band 5. It implies that ionization event from these orbitals is almost equivalent. Then, we related bands 8 and 12 to $3b_{2g}(n_{||})$ and $3b_{3u}(n_{||})$, respectively. The remaining bands 6 and 9 are assigned by the results of OVGF calculations, since the calculation predicted IPs of these bands within 0.1 eV. von Niessen et al.[19] have also proposed the assignment of bands 1−14 based on the theoretical calculation. Although the sequence of orbital characters almost agrees with ours, they did not resolved bands 3−4 and 9−11. Collision-

energy-resolved PIES (CERPIES) of this compound as shown in Figure 6 partially resolved these bands structures, which enable us to refine their bands origins and also to assign these bands more unambiguously. This finding again indicates that the importance and powerfulness of the 2D-PIES study in order to assign the complicated UPS.

Slope parameters of CEDPICS for all bands show negative values. Moreover, slope of each band is almost equivalent to that of the corresponding band for *m*-$C_6H_4F_2$. This finding suggests that the reactivity and interaction of each MO upon the electrophilic attack of the He* atoms is almost equivalent between *m*- and *p*-$C_6H_4F_2$. This is also supported by the theoretical calculations as recognized by the similarity between the calculated interaction potentials of *m*- and *p*-$C_6H_4F_2$ with Li atom as shown in Figures 11 and 12.

Relative Reactivity of Orbitals with Metastable Atoms. In the Penning ionization process, A* can be regarded as an electrophilic reagent, because A* extracts an electron from a MO of M. From this viewpoint, the relative band intensity of PIES is closely related to the reactivity of the corresponding orbital. The reaction probability also depends on anisotropy of interaction potentials, since target MOs have anisotropic electron distributions. In this section, we will discuss the relative reactivity and/or anisotropic interaction around the $\pi_{3,2,1}$, π_F, $n_{||}$, and σ_{CF} orbitals region of difluorobenzenes upon electrophilic attack by metastable helium atoms on the basis of the relative PIES intensities and slope parameters of the $\pi_{3,2,1}$, π_F, $n_{||}$, and σ_{CF} bands in CEDPICS.

(i) Reactivity of the $\pi_{3,2,1}$ Orbitals. It is noted that the PIES intensity of π_2 band is slightly larger than that of the π_3 band for *o*- and *m*-$C_6H_4F_2$, while for *p*-$C_6H_4F_2$ the π_2 band intensity is about two times stronger than the π_3 band intensity. This cannot be explained by the steric shielding effect as was discussed in the case of *p*-C_6H_4Cl.[48] Discrepancy of the reactivity among $\pi_{3,2,1}$ orbitals can be raised from the variation of electron distribution owing to nodal planes around the F atoms. For the purpose of explaining the reactivity of $\pi_{3,2,1}$ orbitals, first, electron distributions (molecule) of these orbitals are segmented as several parts defined by nodal planes, which are schematically drawn as dashed curves in Figures 7−9, and second, we count the number of hydrogen atoms, which have certain electron distribution outside the repulsive surface, faced toward outside in a given segment. Numbers written in italic at each segment in the figures are defined by this procedure. For example, electron distribution of the π_2 orbital of *o*-$C_6H_4F_2$ shown in Figure 7 can be divided into four segments (A, B, C, D) by nodal planes. The number in an A or B segment becomes zero, since there is little electron density around the hydrogen atom. On the other hand, in the case of segments B and C, there are two hydrogen atoms, which have electron distribution outside the repulsive surface, in a given segment. Then the numbers "2" are denoted to the corresponding segments in Figure 7. Similarly, electron distribution of the π_2 orbital of *o*-$C_6H_4F_2$ can be divided into an E and F segment. The number in an E segment becomes zero, while that in a F segment turns out to be "4". These numbers can be used as indices to account for reactivity as follows: (1) the largest number in a given MO indicates the most reactive site and it can be used to compare the reactivity of the other orbitals; the larger number indicates the larger reaction probability, and (2) the summed whole numbers in a given MO is also important to compare reactivity with the other MOs; the larger summed number indicates the larger reaction probability. From the first rule, PIES intensity order $\pi_1 \leq \pi_2 < \pi_3$ of *p*-$C_6H_4F_2$ can be clearly explained since the π_1 and π_2 orbitals have larger numbers "2" than that "1" of the π_3 orbital. It should be noted that drastic intensity difference between π_3 and $\pi_{2,1}$ bands in *p*-$C_6H_4F_2$ implies that the first rule is more dominant than the second one to account for $\pi_{3,2,1}$ orbital reactivity. However, in the case of *o*-$C_6H_4F_2$, importance of the second rule was implied because the observed intensity order $\pi_3 \leq \pi_2$ cannot be explained only from the first rule (π_3 orbital has larger single number "3" than that "2" of π_2). By taking the balance of the first and second rules into account, PIES intensity order $\pi_3 \leq \pi_2 \leq \pi_1$ for *o*-, *m*-$C_6H_4F_2$ can be explained.

(ii) Reactivity of the π_F Orbitals. The PIES intensities of the π_F bands show relatively strong. This is because the π_F orbitals extend outside the molecular surface as indicated at the right side of Figures 7−9. The π_F orbitals were made by the conjugation between the 2p orbital of the C atoms and the 2p orbitals of the F atoms. Then, the electron distribution outside the repulsive surface depends on the magnitude of the conjugation between 2p orbitals of the C and F atoms. There are two π_F orbitals for each compound, which are associated with the u and g combinations of the F 2p orbitals. Two π_F bands for *m*- and *p*-$C_6H_4F_2$ overlapped with each other. Then, it is hardly possible to discuss the relative reactivity for the π_F bands in a given compound. On the other hand, in the case of *o*-$C_6H_4F_2$, two π_F bands are fairly resolved to discuss the relative reactivity, while band 11($1b_1(\pi_F)$) overlapped with neighboring band 12. However, as discussed before, PIES intensity of band 11,12 can be mainly attribute to ionization from $1b_1(\pi_F)$ orbital. Observed larger PIES intensity of band $1b_1(\pi_F)$ compared to the band $1a_2(\pi_F)$ can be explained by larger electron density outside the repulsive surface for the $1b_1(\pi_F)$ orbital. It is noted that this density discrepancy between two π_F orbitals in a given compound can be only found for *o*-$C_6H_4F_2$ because of two adjacent F atoms as shown electron density maps in Figures 7−9. As mentioned in the reactivity of $\pi_{3,2,1}$ orbitals, node effect has to be considered to account for reactivity. This is also applicable to the reactivity of the π_F orbitals and becomes important to compare the relative reactivity of π_F orbitals among these compounds as follows. CEDPICS of the π_F bands showed negative and relatively large absolute values of slope parameters. This observation indicated that ionization from these MOs governed by attractive force. Around the collinear accesses of the He* to C−F bonds can be responsible for this attractive interaction, since the other direction approaches of the He* were predicted to be repulsive. As can be seen in Figure 10(b)-12(b), a wider attractive region was found for *o*-$C_6H_4F_2$, while there are two potential well for *m*- and *p*-$C_6H_4F_2$. Then, two π_F orbitals reactivity for *m*- and *p*-$C_6H_4F_2$ are expected to be similar to each other owing to the restricted reactive He* approach toward each π_F orbital, which is called hereafter as quasi-node effect, while the u combination of two F 2p orbitals gives larger electron distribution outside the repulsive surface than that of g combination. Extraordinary strong PIES intensity of band $1b_1(\pi_F)$, which is generated by the u combination of the F atoms, in comparison with the other π_F orbitals among these compounds is consistent with the above discussion, since there is neither the node effect nor quasi-node effect for this MO. These observations are closely related to the fact that partial ionization cross section depends both upon anisotropy of interaction potential between the He* and molecule and also upon the electron density outside the repulsive surface of the target MO.

(iii) Reactivity of the $n_{||}$ Orbitals. The relative intensities in PIES and slope parameters of $n_{||}$ and σ_{CF} orbitals for each compound were obtained with respect to those of average value

TABLE 4: Relative PIES Intensities and Slope Parameters of $n_{||}$, σ_{CF}, and π_F Bands in *o*-, *m*-, and *p*-$C_6H_4F_2$

compd	$I(n_{\|})/I(\pi)$	$m(n_{\|})/m(\pi)$	$m(\sigma_{CF})/m(\pi)$
o-$C_6H_4F_2$	0.40 ± 0.04	0.90 ± 0.10	1.43 ± 0.20
m-$C_6H_4F_2$	0.36 ± 0.05	0.64 ± 0.11	0.82 ± 0.14
p-$C_6H_4F_2$	0.36 ± 0.05	0.77 ± 0.02	0.97 ± 0.02

of the π_3 and π_2 bands as a reference. Because the π_3 and π_2 orbitals are overlapped with each other for *o*- and *p*-$C_6H_4F_2$, and the whole node effect for π_3 and π_2 orbitals among these compounds seems to be equivalent.

It has been reported that the $n_{||}$ orbital of monofluorobenzene was effectively shielded by the benzene ring and then showed a markedly weak intensity(reactivity) in PIES with a metastable atom.[12] Similar effect has been found in PIES of *o*-, *m*-, *p*-$C_6H_4F_2$; the $n_{||}$ bands are significantly reduced owing to the shielding of the benzene ring. This shielding effect is clearly seen for band 6 in *o*- and *m*-$C_6H_4F_2$ and also for band 5 in *p*-$C_6H_4F_2$ since these bands are not suffering from overlapping with the neighboring bands. Then, to compare the relative intensity and slope parameter of CEDPICS for the $n_{||}$ bands, the ratios $I(n_{||})/I(\pi)$ and $m(n_{||})/m(\pi)$ for these bands are evaluated. We used integrated intensities for these bands in Figures 1-3 after de-convoluting the $n_{||}$ bands from slightly overlapped neighboring bands. Errors for $m(n_{||})/m(\pi)$ were estimated from $m(n_{||})/m(\pi_3)$ and $m(n_{||})/m(\pi_2)$. The values are summarized in Table 4. Obtained ordering of the relative intensity and slope parameter was *o*- > *m*- ~ *p*-$C_6H_4F_2$. It indicates that in the case of *o*-$C_6H_4F_2$ the $n_{||}$ orbital region is less shielded from the attack of metastables by the benzene ring because the close proximate two F atoms in *o*-$C_6H_4F_2$ generates a wider attractive region. Namely, in the case of *o*-$C_6H_4F_2$, the shielding is partly overlapped because the position of substitutes is adjacent. The two atoms, therefore, more or less counteract their shielding effect each other. On the other hand, in *m*- and *p*-$C_6H_4F_2$, this counteracting effect is smaller. It is also noted that well depth and width of attractive potential around each F atoms as shown in Figures 10b, 11b, and 12b is almost identical. As a result, integrated attractive region for each compound is equivalent. These results indicate that attractive effect around the reaction point becomes stronger with increasing the width (spatial extension) of a potential well. This finding is closely related to the large attractive effect around the π orbitals region, which have wider and shallow potential well, and also to the empirical rule (1) as mentioned before.

(iv) Reactivity of the σ_{CF} Orbitals. As a common feature of *o*-, *m*-, and *p*-$C_6H_4F_2$, the σ_{CF} band intensity in PIES is considerably strong compared to the other bands. This is because these orbitals have larger electron distribution exposed along the C−F bond axis. They readily react with the metastable atoms and give stronger band intensities in PIES. In a given molecule, stronger PIES intensity of σ_{CF} orbital (band 14 for *o*-, *m*-$C_6H_4F_2$ and 13 for *p*-$C_6H_4F_2$) than that of the other σ_{CF} orbital (band 13 for *o*-$C_6H_4F_2$, 12 for *m*-$C_6H_4F_2$, and 13 for *p*-$C_6H_4F_2$) can be explained by the electron density outside the repulsive surface. Namely, stronger intensity can be ascribed to the larger electron density outside the repulsive surface again. Although it is apparent that the σ_{CF} orbitals have larger ionization cross section compared to those of the π_3 and π_2 orbitals, unfortunately it is not possible to discuss the relative reactivity within sufficient accuracy based on the relative intensity of $I(\sigma_{CF})/I(\pi)$ among these compounds owing to the overlapping with neighboring bands. On the other hand, relative slope parameters of CEDPICS, $m(\sigma_{CF})/m(\pi)$, are rather reliable in order to compare the relative anisotropic interaction around the F atom, since the CEDPICS of the only central portion for the corresponding peak were picked up with resultant smaller band overlapping. Here, we used the slope parameter of band 14 (σ_{CF}) for these compounds because of their similar electron distributions. As can be seen in Table 4, the value of $m(\sigma_{CF})/m(\pi)$ for *o*-$C_6H_4F_2$ is larger than those for of *m*- and *p*-$C_6H_4F_2$. This indicates that the σ_{CF} band for *o*-$C_6H_4F_2$ show larger attractive interaction with the metastable atoms than the other isomers. Thus, the ordering of the relative slope parameter of the σ_{CF} bands, *o*- > *m*- ~ *p*-, can be explained by the same fashion as in the case of $n_{||}$ orbital reactivity.

VI. Conclusion

In this study, the results of PIES of *o*-, *m*-, *p*-$C_6H_4F_2$ with metastable He*(2^3S) atom were presented. Highly anisotropic interactions around the F atoms are obtained. Around the collinear access of He*(2^3S) to C−F axis for these compounds is more attractive. It is also found that the $\pi_{3,2,1}$ and π_F bands show the attractive interactions for these compounds. Orbital reactivity and its related attractive interaction depend on the electronic factor due to the nodal plane around the F atoms and the conjugation between the benzene ring and the F atoms. Furthermore, we discussed the relative reactivity and magnitude of the attractive interaction of the $n_{||}$ and σ_{CF} bands for *o*-, *m*-, and *p*-$C_6H_4F_2$ upon electrophilic attack by the He* atoms on the basis of the relative peak intensities in PIES and the slope parameters of CEDPICS in the 2D-PIES. It is found that the ordering of the reactivity of the $n_{||}$ and σ_{CF} orbitals and the magnitude of attractive interaction around the F atoms with the metastable atom was found to be *o*- > *m*- ~ *p*-$C_6H_4F_2$. It indicates that attractive effect becomes stronger for a wider attractive potential.

Acknowledgment. This work has been partially supported by a Grant-in-Aid for Scientific Research from the Japanese Ministry of Education, Science, and Culture. K.I. thanks the Japan Society for the Promotion of Science (JSPS) for a JSPS Research Fellowship.

References and Notes

(1) Penning, F. M. *Naturwissenschaften* **1927**, *15*, 818.
(2) Hotop, H.; Niehaus, A. *Z. Phys*. **1969**, *228*, 68.
(3) Ohno, K.; Mutoh, H.; Harada, Y. *J. Am. Chem. Soc*. **1983**, *105*, 4555.
(4) Ohno, K.; Matsumoto, S.; Harada, Y. *J. Chem. Phys*. **1984**, *81*, 4447.
(5) Ohno, K.; Yamakado, H.; Ogawa, T.; Yamata, T. *J. Chem. Phys*. **1996**, *105*, 7536.
(6) Takami, T.; Ohno, K. *J. Chem. Phys*. **1992**, *96*, 6523.
(7) Yamauchi, M.; Yamakita, Y.; Yamakado, H.; Ohno, K. *J. Electron Spectrosc. Relat. Phenom*. **1998**, *88*−*91*, 155.
(8) Kishimoto, N.; Yamakado, H.; Ohno, K. *J. Phys. Chem. A* **1996**, *100*, 8204.
(9) Yamakita, Y.; Yamauchi, M.; Ohno, K. *Chem. Phys. Lett*. **2000**, *322*, 189.
(10) Kishimoto, N.; Ohno, K. *J. Phys. Chem. A* **2000**, *104*, 6940.
(11) Kishimoto, N.; Furuhashi, M.; Ohno, K. *J. Electron Spectrosc. Relat. Phenom*. **2000**, *113*, 35.
(12) Imura, K.; Kishimoto, N.; Ohno, K. *J. Phys. Chem*. *A* **2001**, *105*, 4189.
(13) Fujisawa, S.; Ohno, K.; Masuda, S.; Harada, Y. *J. Am. Chem. Soc*. **1986**, *108*, 6505.
(14) Clark, I. D.; Frost, D. C. *J. Am. Chem. Soc*. **1967**, *89*, 244.
(15) Klessinger, M. *Angew. Chem., Intern. Ed*. **1972**, *11*, 525.
(16) Gilbert, R.; Sandorfy, C. *Chem. Phys. Lett*. **1974**, *27*, 457.
(17) Narayan, B.; Murrell, J. N. *Mol. Phys*. **1970**, *19*, 169.
(18) Palmer, M. H.; Moyes, W.; Spiers, M.; Ridyard, J. N. A. *J. Mol. Struct*. **1978**, *49*, 105.
(19) von Niessen, W.; Diercksen, G. H. F.; Cederbaum, L. S. *Chem. Phys. Lett*. **1977**, *45*, 295.
(20) Streets, D. G.; Ceasar, G. P. *Mol. Phys*. **1973**, *26*, 1037.

(21) Sell, J. A.; Mintz, D. M.; Kuppermann, A. *Chem. Phys. Lett*. **1978**, *58*, 601.
(22) Bieri, G.; Åsbrink, L.; von Niessen, W. *J. Electron Spectrosc. Relat. Phenom*. **1981**, *23*, 281.
(23) Aoyama, M. Ph.D. Thesis, University of Tokyo, 1989.
(24) Mitsuke, K.; Takami, T.; Ohno, K. *J. Chem. Phys*. **1989**, *91*, 1618.
(25) Ohno, K.; Takami, T.; Mitsuke, K.; Ishida, T. *J. Chem. Phys*. **1991**, *94*, 2675.
(26) Takami, T.; Mitsuke, K. Ohno, K. *J. Chem. Phys*. **1991**, *95*, 918.
(27) Gardner, J. L.; Samson, J. A. R. *J. Electron Spectrosc. Relat. Phenom*. **1976**, *8*, 469.
(28) Kimura, K.; Katsumata, S.; Achiba, Y.; Yamazaki, T.; Iwata, S. *Handbook of He I Photoelectron Spectra of Fundermental Organic Molecules*; Japan Scientific: Tokyo, 1981.
(29) Turner, D. W.; Baker, C.; Baker, A. D.; Brundle, C. R. *Molecular Photoelectron Spectroscopy*; Wiley: London, 1970.
(30) Yee, D. S. C.; Stewart, W. B.; Mcdowell, C. A.; Brion, C. E. *J. Electron Spectrosc. Relat. Phenom*. **1975**, *7*, 93.
(31) Hotop, H.; Hubler, G. *J. Electron Spectrosc. Relat. Phenom*. **1977**, *11*, 101.
(32) (a) Auerbach, D. J. *Atomic and Molecular Beam Methods*; Scoles, G., Ed.; Oxford University: New York, 1988; p 369. (b) Kishimoto, N.; Aizawa, J.; Yamakado, H.; Ohno, K. *J. Phys. Chem. A* **1997**, *101*, 5038.
(33) Doraiswamy, S.; Sharma, S. *J. Mol. Struct.* **1983**, *102*, 81.
(34) Domenicano, A.; Schultz, G.; Hargittai, I. *J. Mol. Struct.* **1982**, *78*, 97.
(35) Pauling, L.; *The Nature of Chemical Bond*; Cornell University: Ithaca, New York, 1960.
(36) Rothe, E. W.; Neynaber, R. H.; Trujillo, S. M. *J. Chem. Phys*. **1965**, *42*, 3310.
(37) Illenberger, E.; Niehaus, A. *Z. Phys. B* **1975**, *20*, 33.
(38) Parr, T.; Parr, D. M.; Martin, R. M. *J. Chem. Phys*. **1982**, *76*, 316.
(39) Hotop, H. *Radiat. Res*. **1974**, *59*, 379.
(40) Haberland, H.; Lee, Y. T.; Siska, P. E. *Adv. Chem. Phys*. **1981**, *45*, 487.
(41) Frisch, M. J.; Trucks, G. W.; Schlegel, H. B.; Scuseria, G. E.; Robb, M. A.; Cheeseman, J. R.; Zakrzewski, V. G.; Montgomery, J. A., Jr.; Stratmann, R. E.; Burant, J. C.; Dapprich, S.;. Millam, J. M; Daniels, A. D.; Kudin, K. N.; Strain, M. C.; Farkas, O.; Tomasi, J.; Barone, V.; Cossi, M.; Cammi, R.; Mennucci, B.; Pomelli, C.; Adamo, C.; Clifford, S.; Ochterski, J.; Petersson, G. A.; Ayala, P. Y.; Cui, Q.; Morokuma, K.; Malick, D. K.; Rabuck, A. D.; Raghavachari, K.; Foresman, J. B.; Cioslowski, J.; Ortiz, J. V.; Baboul, A. G.; Stefanov, B. B.; Liu, G.; Liashenko, A.; Piskorz, P.; Komaromi, I.; Gomperts, R.; Martin, R. L.; Fox, D. J.; Keith, T.; Al-Laham, M. A.; Peng, C. Y.; Nanayakkara, A.; Challacombe, M.; Gill, P. M. W.; Johnson, B.; Chen, W.; Wong, M. W.; Andres, J. L.; Gonzalez, C.; Head-Gordon, M.; Replogle, E. S.; Pople, J. A. Gaussian, Inc.: Pittsburgh, PA, 1998.
(42) von Niessen, W.; Schirmer, J.; Cederbaum, L. S. *Comput. Phys. Rep*. **1984**, *1*, 57.
(43) (a) Zakrzewski, V. G.; Ortiz, J. V. *Int. J. Quantum Chem. Symp*. **1994**, *28*, 23. (b) Zakrzewski, V. G.; Ortiz, J. V. *Int. J. Quantum Chem.* **1995**, *53*, 583.
(44) Ohno, K.; Imai, K.; Matsumoto, S.; Harada, Y. *J. Phys. Chem*. **1983**, *87*, 4346.
(45) Munakata, T.; Harada, Y.; Ohno, K.; Kuchitsu, K. *Chem. Phys. Lett*. **1981**, *84*, 6.
(46) Ohno, K.; Fujisawa, S.; Mutoh, H. Harada, Y. *J. Phys. Chem*. **1982**, *86*, 440.
(47) Harada, Y.; Ohno, K.; Mutoh, H. *J. Chem. Phys*. **1983**, *79*, 3251.
(48) Fujisawa, S.; Oonishi, I.; Masuda, S.; Ohno, K.; Harada, Y. *J. Phys. Chem*. **1991**, *95*, 4250.
(49) Masuda, S.; Aoyama, M.; Ohno, K.; Harada, Y. *Phys. Rev. Lett*. **1990**, *65*, 3257.
(50) Frueholz, R. P.; Flicker, W. M.; Mosher, O. A.; Kuppermann, A. *J. Chem. Phys*. **1979**, *70*, 3057.